C. R. Physique 15 (2014) 140–150

Contents lists available at ScienceDirect

Comptes Rendus Physique

www.sciencedirect.com

Electron microscopy / Microscopie électronique

Seeing and measuring in 3D with electrons

Voir et mesurer dans l'espace 3D avec des électrons

Sara Bals *, Bart Goris, Thomas Altantzis, Hamed Heidari, Sandra Van Aert, Gustaaf Van Tendeloo

EMAT, University of Antwerp, Groenenborgerlaan 171, B-2020 Antwerp, Belgium

ARTICLE INFO

Article history:
Available online 20 January 2014

Keywords:
Electron tomography
Atomic resolution
Three-dimensional reconstruction
Nanostructures

Mots-clés :
Tomographie électronique
Résolution atomique
Reconstruction en trois dimensions
Nanostructures

ABSTRACT

Modern TEM enables the investigation of nanostructures at the atomic scale. However, TEM images are only two-dimensional (2D) projections of a three-dimensional (3D) object. Electron tomography can overcome this limitation. The technique is increasingly focused towards quantitative measurements and reaching atomic resolution in 3D has been the ultimate goal for many years. Therefore, one needs to optimize the acquisition of the data, the 3D reconstruction techniques as well as the quantification methods. Here, we will review a broad range of methodologies and examples. Finally, we will provide an outlook and will describe future challenges in the field of electron tomography.

RÉSUMÉ

L'évolution récente des MET permet d'explorer les nanostructures à l'échelle de l'atome. Cependant, les images obtenues ne sont que des projections bidimensionnelles d'objets 3D. La tomographie électronique permet de pallier cette limitation et se concentre de plus en plus sur les mesures quantitatives. De plus, la résolution atomique en 3D représentait depuis longtemps le but ultime en tomographie. Il est donc nécessaire d'optimiser l'acquisition des données, les techniques de reconstruction 3D ainsi que les méthodes de quantification. Nous allons passer en revue différentes méthodologies et exemples. Nous discuterons ensuite des perspectives et des nouveaux défis à relever dans ce domaine.

1. Introduction

Modern transmission electron microscopy (TEM) is the ideal technique for the characterization of (nano)materials. However, it is important to point out that TEM images are only two-dimensional (2D) projections of three-dimensional (3D) objects. To overcome this problem, 3D electron microscopy or so-called "electron tomography" was developed. This technique has been used successfully in the field of biology for several decades [1,2], but the resolution is limited to the nanometre range because of several parameters such as beam damage, the thickness of the sample and the sample preparation [3]. Also the use of highly defocused images in order to improve phase contrast will form a limiting factor [4]. For inorganic materials, beam damage might be a bottleneck for some samples, but there are more important problems to

* Corresponding author. Tel.: +32 (0)32653284.
E-mail address: sara.bals@ua.ac.be (S. Bals).

1631-0705/$ – see front matter
http://dx.doi.org/10.1016/j.crhy.2013.09.015

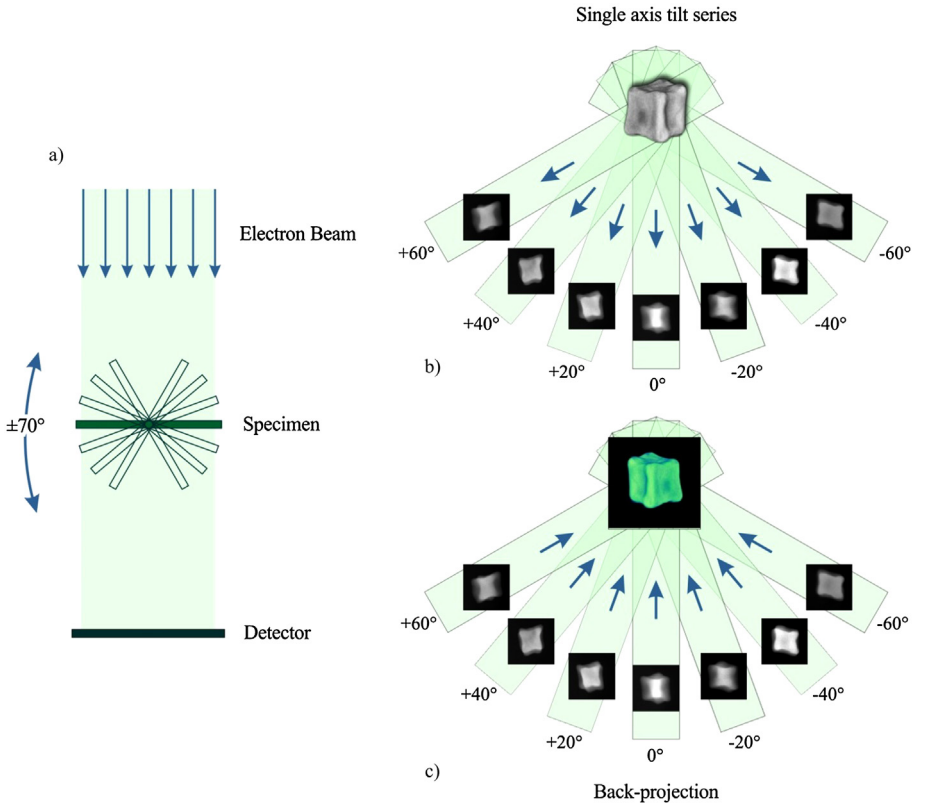

Fig. 1. (Color online.) A schematic illustration of a continuous electron tomography experiment, including the acquisition of a tilt series (a) and (b) and back projection of the images along their original acquisition directions (c).

overcome. Conventional bright field TEM images of crystalline materials are often dominated by Bragg scattering and for certain orientations, the interaction is non-linear. This violates the so-called "projection requirement", which states that each image of a tilt series for electron tomography should be a monotonic projection of a physical property of the sample under investigation [5]. In the field of materials science, electron tomography was therefore initially only used for polymers [6] and porous materials [7]. After the combination of high angle annular dark field scanning transmission electron microscopy (HAADF STEM) and electron tomography, which was demonstrated by Midgley et al. [8], electron tomography became a standard method to characterize inorganic materials as well.

Over the years, a broad range of electron microscopy techniques such as bright field TEM (BF TEM), HAADF STEM, annular dark field TEM, electron holography and energy filtered TEM (EFTEM) and energy dispersive X-ray spectroscopy (EDX) have all been extended to 3D, providing a world of new information on structure function relationships across a broad range of samples and applications [9–17]. In addition to the demand for quantitative electron tomography, the ultimate goal has been to achieve electron tomography with atomic resolution. Although this is not yet a standard possibility for all structures, significant progress has recently been achieved.

2. Conventional electron tomography

When using conventional electron tomography (see Fig. 1), also referred to as "continuous electron tomography", a tilt series of TEM images is acquired by tilting the sample over a large tilt range, with an increment of typically 1 or 2°. After alignment of the projection images, using e.g. cross-correlation, the tilt series is combined into a 3D reconstruction of the original object through a mathematical algorithm. When applying for example "direct back projection" [2,18], the images of the tilt series are back projected along the original acquisition angles. In order to correct for an uneven sampling of the spatial frequencies, a weighting filter is often used. This technique is referred to as "weighted back projection" and is the most commonly used reconstruction algorithm. With the increase of computing power, iterative reconstruction techniques such as e.g. the simultaneous iterative reconstruction technique (SIRT) became widely used [19]. These algorithms improve the quality of the reconstruction in an iterative manner by minimizing the difference between the original projection images and forward projections of the intermediate reconstructions.

Using the conventional approach, the quality of such a reconstruction is predominantly determined by the number of projections. Unfortunately, it is mostly impossible to tilt the sample over the full 360°, since there is only limited spacing for the sample holder in between the objective pole pieces of the microscope or because of shadowing effects that occur at

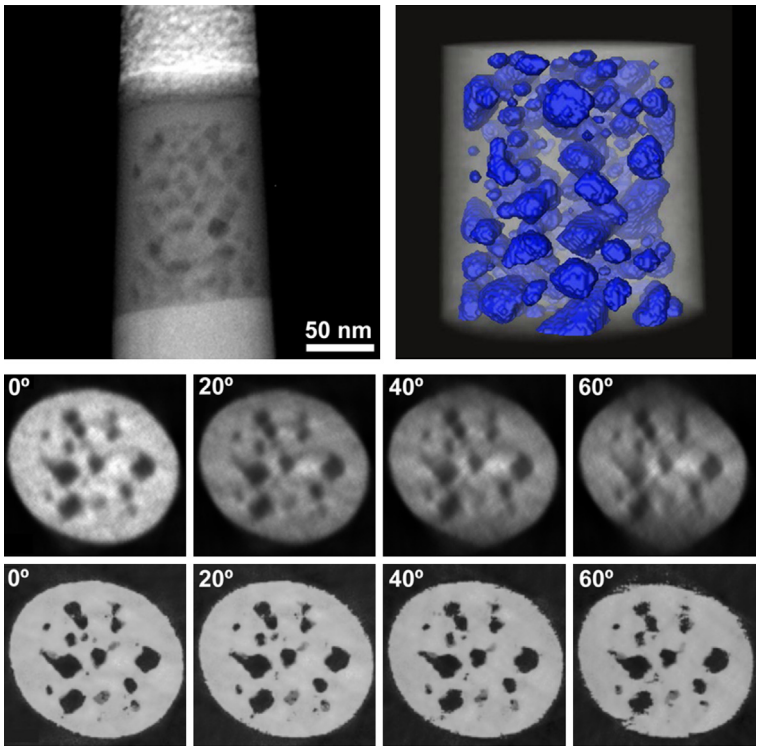

Fig. 2. (Color online.) Top left: 2D projection image of a needle-shaped pillar, obtained for a porous layer of $La_2Zr_2O_7$. The visualization of the 3D reconstruction is shown on the right. Orthoslices through the reconstruction are also presented as a function of increasing missing wedge. The reconstructions are based on a SIRT reconstruction (top) and a discrete tomography reconstruction as explained in Section 3.2 (bottom).

higher tilt angles. When using a dedicated, single tilt tomography holder, a tilt range of typically $\pm 80°$ can be covered. The consequent lack of projection images for a certain range of angles leads to a so-called "missing wedge" of information [8]. Missing wedge artefacts will heavily influence the quality and resolution of the reconstruction. This loss of resolution can be particularly observed along the axes perpendicular to the tilt axis. In addition to missing wedge artefacts, it can be expected that a limited sampling and slight misalignments will also negatively influence the quality of the reconstruction. Boundaries between areas with a different composition will be blurred and this may hamper a reliable qualitative visualization as well as an accurate quantification of the reconstructed object.

3. Quantitative electron tomography

3.1. Acquisition

The demand in the field of electron tomography is increasingly focused towards quantitative measurements of morphologies, chemical compositions or even properties. In order to reach these goals, one needs to optimize the acquisition of the data, the 3D reconstruction techniques (including the alignment procedures) as well as the post processing and the quantification methods.

Due to the missing wedge, the resolution is anisotropic and inferior along the direction where the information is missing. In order to improve the quality and the resolution of a 3D reconstruction, based on continuous electron tomography, it is therefore necessary to overcome missing wedge artefacts as much as possible. Therefore, new types of tomography sample holders were developed and subsequent acquisition schemes were proposed. For example, "dual-axis tilt electron tomography" is an approach in which a second tilt series is acquired along a tilt axis, perpendicular to the tilt axis of the first series. In this manner, the missing wedge is reduced to a missing pyramid, which leads to an improvement of the quality of the 3D reconstruction [20,21]. An alternative is so-called "on-axis tilt tomography", which is based on the use of a needle-shaped sample that is prepared by focused ion beam (FIB) milling. The needle, having a diameter of approximately 100–300 nm, is attached to a dedicated holder and enables one to rotate the needle over a tilt range of 360° eliminating missing wedge artefacts [22–24]. An example of a study in which on-axis tilt tomography is used, is presented in Fig. 2. In this study, a porous $La_2Zr_2O_7$ layer was investigated [23,25]. Orthoslices through a 3D reconstruction based on a full tilt series acquired using a needle-like sample show that missing wedge effects are absent. The effect of the missing wedge is furthermore illustrated in Fig. 2, where 3D reconstructions are presented that are obtained by eliminating a range of projections from the original tilt series. The approach is directly applicable to samples for which a needle-shaped sample can be

prepared (e.g. by FIB). In addition, there have been studies in which the technique was also applied to image nanoparticles in 3D. For such experiments, one needs to alter the rotation stub of the tomography holder [26].

Although the missing wedge is completely eliminated when using on-axis tilt tomography, quantification is still far from straightforward and it is furthermore unlikely that the approach might lead to atomic resolution in 3D in a straightforward manner. One important bottleneck is the thickness of the needle: when decreasing the diameter, required to obtain high resolution (S)TEM projection images, the stability of the sample during the tilt series will be a limiting factor.

Although it is clear that approaches in which the missing wedge is minimized can be thought of as a crucial step towards quantification in 3D [23], there are still only a limited number of examples of quantitative analysis performed in the field of electron tomography [23,27–29]. One of the remaining challenges is that a segmentation step is required to determine the correspondence between different greyscales in the reconstruction and different compositions (or features) in the original structure. Segmentation is often performed manually but this approach is clearly very time consuming and can be subjective. Segmentation is heavily influenced by artefacts related to the missing wedge and it was found that samples need to be tilted over a range of at least $\pm 80^\circ$ in order to obtain reliable quantitative measurements [22,23]. However, even if projection images could be acquired for a full range of angles, several other minor reconstruction artefacts such as the effect of a limited sampling and slight misalignments [8] might still be present and will hamper the segmentation step. Recent progress concerning alignment procedures was made by using the contrast observed in the tomogram as a criterion to iteratively optimize the alignment of the tilt series [30].

Another bottleneck on the route to quantitative electron tomography might be the so-called cupping artefact, which corresponds to an underestimation of the intensities at the interior of a HAADF STEM reconstruction [31]. This artefact is due to the non-linearity of the HAADF STEM signal and is especially apparent for samples having a large thickness such as nanoparticle assemblies [32]. Novel segmentation procedures have recently been proposed [33], but in general, a quantitative interpretation based on the conventional reconstruction algorithms remains difficult.

3.2. Reconstruction

None of the algorithms described above uses additional information on the system that one wants to reconstruct. By implementing *a priori* knowledge, the quality of a reconstruction can be drastically improved and very often, such additional information on the sample is indeed available or can be obtained using other (TEM) techniques. One approach to incorporate *a priori* knowledge is by using "discrete tomography" as implemented in the discrete algebraic reconstruction algorithm (DART). DART is an iterative algorithm that alternates between steps of the SIRT algorithm from continuous tomography and certain discretization steps [34,35]. Both for BF TEM and HAADF STEM tomography it was shown that missing wedge artefacts are significantly reduced [34,36]. Another advantage is that segmentation of the 3D dataset is carried out during the reconstruction in a reliable and objective manner [23]. This is illustrated in Fig. 2 where the quality of the SIRT reconstruction rapidly decreases with increasing missing wedge, but the discrete tomography reconstruction, obtained using DART, still shows a good (qualitative) agreement with the results obtained for a full tilt range. These results furthermore showed that it is possible to obtain reliable and quantitative results using the DART algorithm, even for a tilt range as limited as $\pm 60^\circ$ [23].

A different kind of prior knowledge is exploited when using compressive sensing based reconstruction algorithms [37–39]. A specific variant of this approach is "Total Variation Minimization" (TVM), where it is assumed that the object that needs to be reconstructed has a sparse gradient at the nanometre scale. For objects at the nanoscale, it is indeed often a good assumption that boundaries between different compounds are sharp, leading to a sparse gradient of the object. TVM again has the advantage that the resulting 3D reconstructions suffer less from the missing wedge. In a recent study, a combination of TVM and discrete tomography was proposed. The threshold intensities from a TVM reconstruction hereby serve as the grey values that are requested for a discrete reconstruction [40].

Clearly both DART and TVM are very promising algorithms when quantitative measurements in 3D are aimed at. Recently, it was also demonstrated that it is possible to incorporate prior knowledge on the geometry of the sample, such as convexity and homogeneity, during the 3D reconstruction [41]. In the majority of the studies where these advanced reconstruction algorithms have been applied so far, a resolution in the nanometre range was obtained. Nevertheless, it is clear that these algorithms will also play a key role when atomic resolution in 3D is the final goal.

4. Seeing atoms in three dimensions

Despite all of the progress that was made towards improving the ability to obtain quantitative results, atomic resolution in 3D remained the ultimate goal in the field of electron tomography for many years [12,42]. The underlying theory for atomic resolution tomography has been well-understood [42,43], but nevertheless, experimental results were lacking until recently, when significant progress, pushing the resolution in 3D to the atomic level, was achieved using different methodologies [44–47].

A first approach is based on the acquisition of a limited number of HAADF STEM images that are acquired along different zone axes. As shown in Fig. 3, a 3D reconstruction at the atomic scale could be obtained for an Ag nanoparticle with a diameter of approximately 3 nm, embedded in an Al matrix [44]. The reconstruction was based on only 2 HAADF STEM

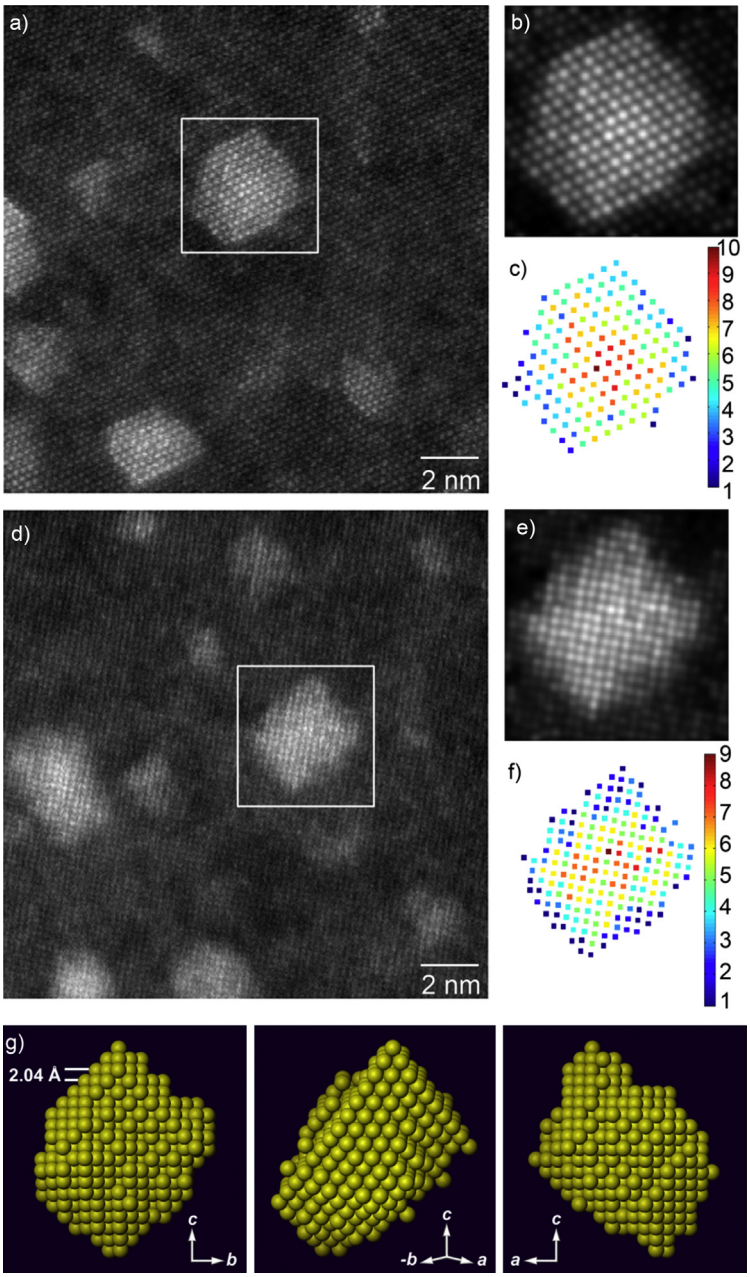

Fig. 3. (Color online.) (a) Experimental HAADF STEM image of nanosized Ag clusters embedded in an Al matrix in [10$\bar{1}$] zone-axis orientation. (b) Refined parameterized model of the boxed region of (a). (c) Number of Ag atoms per column. (d) Experimental image in [100] zone-axis orientation. (e) Refined model of the boxed region of (d). (f) Number of Ag atoms per column. (g) Computed 3D reconstruction of the Ag nanocluster viewed along three different directions.

images obtained when viewing the same particle along the [10$\bar{1}$] and the [100] zone-axes (see Figs. 3(a) and 3(d), respectively). Using advanced statistical parameter estimation theory, the parameters of an empirical physics-based model have been estimated in the least squares sense. The refined models are shown in Figs. 3(b) and 3(e) for the particles shown in the white boxed regions of Figs. 3(a) and 3(d). The estimated parameters could be exploited to count the number of atoms in a column with single atom precision [44,48]. The resulting counting results are shown in Figs. 3(c) and 3(f) and have been used as an input for discrete tomography. In contrast to the approach explained in Section 3.2, we will not use the number of expected grey levels in the final reconstruction as an input for 3D reconstruction. For reconstructions at the atomic scale, the following prior knowledge is incorporated: (i) all of the atoms lie on a face-centred-cubic (fcc) grid; (ii) the particle is connected and contains no holes; (iii) the number of edges should be minimized. The computed 3D reconstruction of the

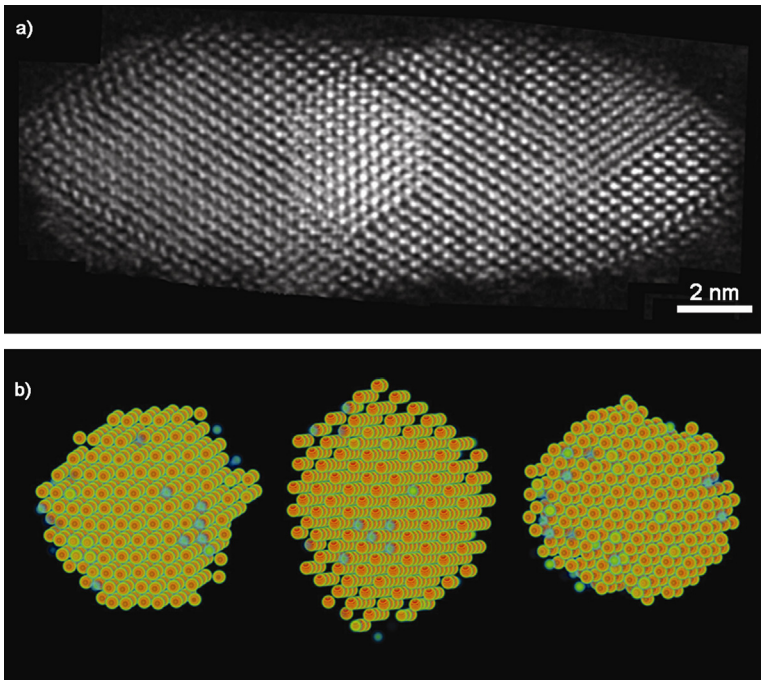

Fig. 4. (Color online.) (a) 2D HAADF STEM image of a PbSe–CdSe core–shell structure. (b) Different viewing directions of the 3D reconstruction of the Pb lattice forming the core of the nanorod.

Ag nanocluster viewed along three different directions is shown in Fig. 3(g). An excellent match was found when comparing the 3D reconstruction with additional projection images that were acquired along additional zone axes.

Although the technique was experimentally first applied to nanocrystals present in a stabilizing matrix, the approach is definitely more generally applicable and can also be used to study free-standing nanocrystals. Fig. 4, for example, illustrates the result of a study that was performed for colloidal core–shell semiconductor nanocrystals [45]. Using the atom counting procedure, the number of Pb atoms in the core could be quantified for [110, 100], and [010] zone axes projections. Next, discrete tomography is used to reconstruct the occupancies of the Pb positions in 3D. The resulting reconstruction is presented along different viewing directions in Fig. 4(b). The symmetry of the core is clearly different from what could be expected based on a single 2D image.

The discrete approach explained above assumes that the atoms are positioned on a (fixed) face-centred-cubic lattice and that the particle contains no holes. These assumptions provide an excellent start for the investigations described above, but deviations from a fixed grid, caused by defects, strain or lattice relaxation might be important parameters that determine the physical properties of nanomaterials. One may therefore wonder if continuous tomography can lead to visualization of individual atoms in case the projection images yield atomic resolution. Fullerene-like nanostructures were investigated with a sub-nanometre spatial resolution $(0.3 * 0.6 * 0.6)$ nm^3 by Bar Sadan and co-workers [12]. In this work, a tilt series was recorded with a tilt range of $\pm 60^\circ$ and a fixed 3° increment. The series was acquired in BF TEM mode using a microscope aligned at negative Cs imaging conditions. The tomographic reconstruction, which was obtained for MoS_2 octahedral nanoparticles could indeed be interpreted in terms of the atomic structure.

More recently, Scott et al. reported to have obtained a 3D reconstruction at a resolution of 0.24 nm. An icosahedral multiply twinned Au nanoparticle with a diameter of $\sim$10 nm was hereby investigated [46]. Although not all atoms could be located in this reconstruction, the authors conclude that individual atoms could be observed in some parts of the nanoparticle. The reconstruction was obtained without using any prior information and was based on the so-called equally-sloped tomography approach [49]. This means that rather than using a tilt series based on an equal tilt increment, increments in the acquired series are based on angles having equal slopes. In total 69 images were required to obtain this 3D reconstruction. Using the methodology reported by Scott et al. [46], no prior knowledge is assumed, but a relatively large number of images is necessary and not all atoms in the nanoparticle could be visualized. This might be related to the presence of the missing wedge, which will also play an important role for reconstructions at the atomic scale. More recently, the technique was also applied to platinum nanoparticles in which dislocations are present [50].

An alternative approach, based on compressive sensing was recently reported [51]. The advantages of compressive sensing for electron tomography with nanoscale resolution are summarized elsewhere in this paper [37,38], but the technique also holds great promise for 3D reconstructions at the atomic scale. For such reconstructions, one possibility is to exploit the sparsity of the object since only a limited number of voxels in the reconstruction are expected to contain an atom and most voxels will correspond to vacuum [51]. An important advantage of this approach is that the actual positions of

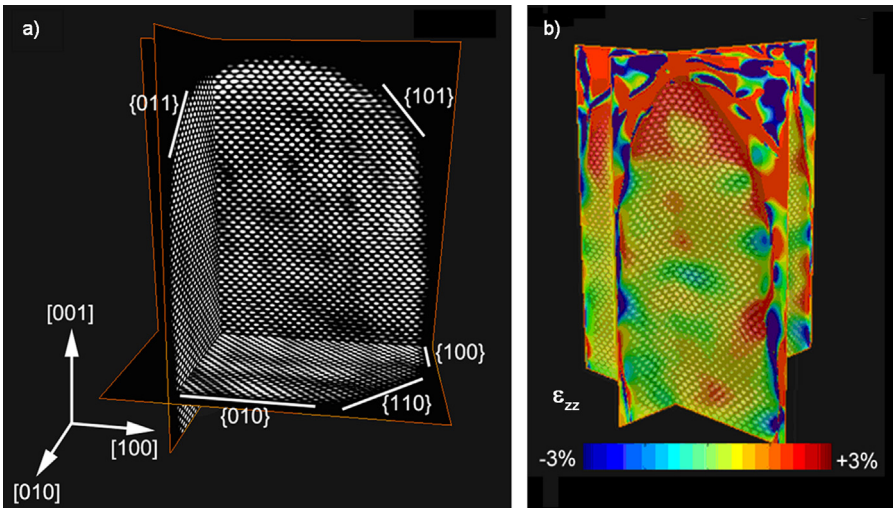

Fig. 5. (Color online.) (a) Three orthogonal slices through the reconstruction of a Au nanorod, showing individual atom positions. The facets composing the morphology can be determined. (b) Slices through the 3D ε_{zz} strain measurement indicate an outward relaxation of the atoms at the tip of the nanorod.

the atoms can be revealed without using any assumptions concerning the crystal lattice. Another benefit is that because of the incorporation of sparsity during the reconstruction, a limited number of projections are sufficient to create a faithful reconstruction of the atomic lattice.

Mathematically, a tomographic reconstruction corresponds to reconstructing an object x starting from its projections b, which are acquired by a projection operator A. The tomographic reconstruction then often corresponds to iteratively solving the following minimization problem.

$$\hat{x} = \arg\min_x \|Ax - b\|_2^2$$

When implementing compressive sensing, an additional penalty parameter λ is introduced leading to a simultaneous minimization of the projection error and the L1-norm of the object (i.e. the sum of the absolute values of all the voxels in the reconstructed object) [52]:

$$\hat{x} = \arg\min_x \left[\|Ax - b\|_2^2 + \lambda\|x\|_1\right]$$

The methodology was applied for Au nanorods and the results are presented in Fig. 5. In order to obtain the 3D reconstruction, 4 different high resolution HAADF STEM images were acquired along different zone axes. Alignment of the images was based on a centre of mass calculation for each projection [46]. The reconstructions were calculated using the iterative algorithm based on compressive sensing as explained above. In Fig. 5(a), orthoslices through the reconstruction of an Au nanorod are presented and it is clear that the fcc crystal lattice of the rod has been reproduced without using prior knowledge on the atomic structure. From these reconstructions, the boundary as well as the tip facets of the rod have been precisely identified and also atomic steps at the surface can be detected. Recently, the technique was combined with statistical parameter estimation theory and was applied to bimetallic nanoparticles. To the best of our knowledge, this is the first experiment in which the atom type of individual atoms in a heterostructure is determined in 3D [53].

A completely different approach that has gained interest with respect to reaching atomic resolution in 3D is by exploiting the reduced depth of focus for aberration corrected HAADF STEM. When the convergence angle is increased to 30 mrad or more, only very thin slices of a sample can be brought into focus at the same time. In this manner, the technique that is referred to as “depth sectioning” can be used to obtain 3D information on a sample. Because of the high signal-to-noise ratio of an aberration corrected microscope it is even possible to detect individual impurity atoms inside the volume of a TEM sample [54]. A drawback of the technique is a strong elongation effect, sometimes larger than a factor of 30, that is present along the electron beam direction for a typical aberration corrected STEM setup [55]. To overcome this problem, a parameter based reconstruction algorithm has been proposed [56] using prior knowledge about the constituent atom types and the microscope settings. Theoretically, it is shown that the resolution can be pushed to the atomic level in all three dimensions and that the positions of all atoms can be retrieved. By using scanning confocal electron microscopy (SCEM), a technique in which the collection optics (of a double aberration corrected TEM) is arranged symmetrically to the illumination optics, the elongation might be significantly reduced [57]. The potential of different S/TEM based techniques was investigated theoretically and it was hereby concluded that energy filtered SCEM (EFSCEM) is the most promising approach, especially in combination with correction of the chromatic aberration [55,58,59].

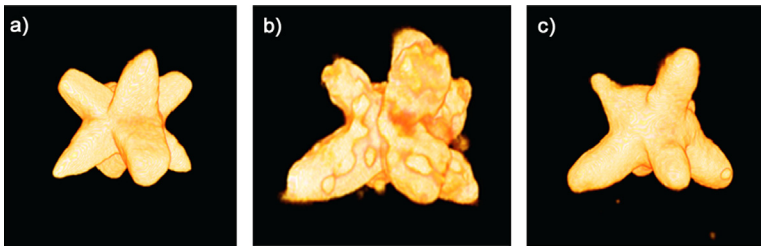

Fig. 6. (Color online.) 3D reconstruction of a CdSe–CdS core–shell octapod at (a) room temperature, (b) 300 °C and (c) 500 °C. Different tips behave in a different manner during heating.

5. Measuring properties in 3D

Electron tomography is no longer based on BF TEM or HAADF STEM images only and has been combined with a broad range of TEM techniques. Incoherent BF STEM was proposed for thick samples [60] and dark-field transmission electron microscopy (ADF TEM) [17], hollow cone illumination [61] or precession techniques [62] have been used to reduce the unwanted diffraction contrast in TEM mode. Other techniques on the other hand, exploit diffraction contrast, e.g. weak-beam dark-field images have been used to reconstruct the 3D network of dislocations in GaN [63]. Furthermore different inelastic TEM techniques are widely used for 3D studies. EFTEM tomography can be carried out with a resolution in the nanometre range [14,64,65]. Plasmon excitation energies have been used for 3D reconstructions of a carbon nanotube encased in nylon [16] and to visualize the distribution of Si nanoparticles embedded in a Si matrix [66]. Also preliminary results on mapping surface plasmons in 3D have also been reported [67].

The combination of electron holography and tomography leads to the possibility to map electric and magnetic fields inside nanostructures in 3D. As described elsewhere in this issue, electron holography enables one to extract the projected scalar potential for electrostatic fields and/or a projected component of the vector potential for magnetic fields. By extending this approach to 3D, the internal electric potential of semiconductor p–n junctions could be characterized with nanometre resolution [11,68]. Mapping magnetic induction is more complicated and rather than using scalar-based tomography (which is based on the projection requirement), vector field electron tomography should be applied. Besides electron holography, also Lorentz TEM can be used to reconstruct the magnetic induction $\mathbf{B}(\mathbf{r})$ or equivalently, the vector potential $\mathbf{A}(\mathbf{r})$. Although the theory behind vector-based tomography is well understood, the experimental combination with TEM is not straightforward [69,70]. One of the main reason is that several tilt series have to be acquired along perpendicular axes in order to reconstruct the field that changes not only in size but also in direction. First experimental results, characterizing the 3D vector potential in and around a magnetic permalloy structure, demonstrate the feasibility and the importance of expanding magnetic measurements by TEM from 2D to 3D [71].

In addition to the 3D characterization of electromagnetic fields, it is also of great importance to measure strain in 3D. It has been shown that using dark field holographic techniques, strain can be measured in 2D with a spatial resolution in the nanometre scale [72]. Current semiconductor science however, requires (quantitative) strain measurements to be in 3D. Also for nanoparticles, in which the fraction of surface atoms with respect to the total number of atoms in the particle becomes considerable, it is of great importance to investigate for example surface relaxation in 3D. Extending state-of-the-art techniques to measure strain also in 3D is not straightforward since 2D strain maps do not fulfill the projection requirement. Again, vector field electron tomography might be able to overcome this problem. Another option is to use the outcome of 3D reconstructions at the atomic scale as an input for techniques such as the geometrical phase analysis [73]. The atom positions are not fixed during the 3D reconstruction presented in Fig. 5 meaning that the reconstruction can serve as a starting point for many other investigations such as ab initio calculations or even strain measurements. As an example, we applied geometrical phase analysis (GPA) [73] to the 3D reconstruction shown in Fig. 5(a) and the result is presented in Fig. 5(b). From this figure is it clear that strain measurements on a local scale can now be carried out in 3D. A reference region where no strain is present, was selected in the middle of the nanorod. This implies that all strain measurements are relative with respect to this reference region. As discussed in [51], an accuracy of 1.3% was found for the results in Fig. 5(b). It can be expected that better accuracies will be reached by combining 3D reconstruction such as the ones in Fig. 5 with statistical parameter estimation theory.

When incorporating nanomaterials in actual devices, they will be exposed to environmental conditions. It is therefore of great interest to perform dynamical 3D studies (e.g. as a function of temperature or when applying strain) by electron tomography as well. Especially for catalysis or optoelectronics, nanoparticle shape dynamics plays an important role. In order to reach these goals, further optimization of tomography holders and reconstruction algorithms will be required. Morphology changes that occur for a branched semiconductor nanostructure, having blunt and sharp tips, were investigated for samples that were heated to different temperatures prior to their investigation in the TEM. The results are illustrated in Fig. 6. 3D experiments in which heating is performed *in-situ* are soon to be expected [74].

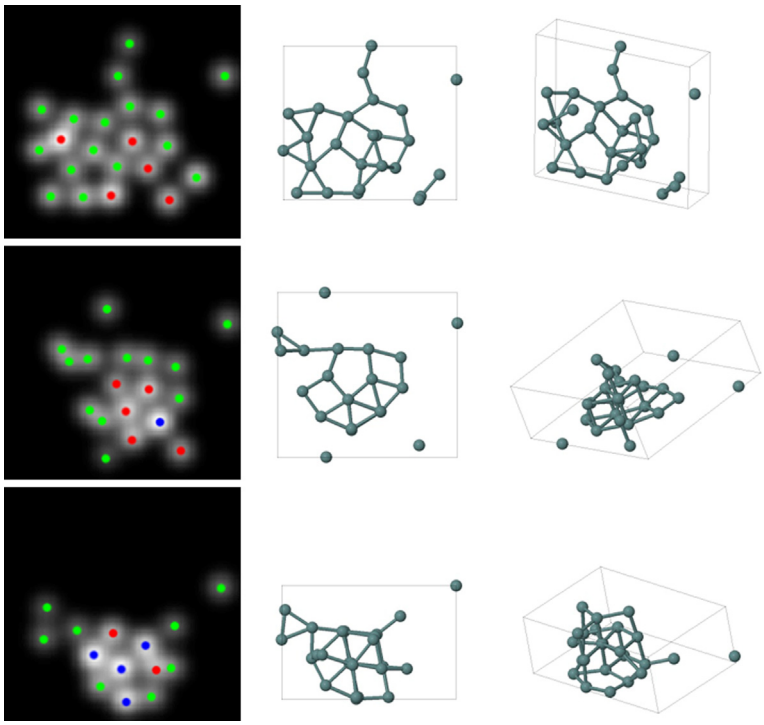

Fig. 7. (Color online.) The left column presents the counting results obtained for 3 different configurations of a single ultra-small Ge cluster. Green, red and blue dots correspond to 1, 2 and 3 atoms respectively. The 3D results of the ab initio calculations are shown at right along different viewing directions.

6. Small, smaller, smallest

All of the abilities and 3D reconstruction tools described above will certainly play an important role in the further characterization of nanostructures. However, we are always confronted with even more challenging samples that force us to push the limits even further. An example of such a material consists of ultra-small nanoparticles or clusters, having sizes below 1 nm. The main bottleneck hampering a 3D investigation at the atomic scale is that these clusters may rotate or show structural changes during investigation by TEM [75]. As a consequence of this dynamical behavior none of the electron tomography methods described in this paper can be applied. On the other hand, the intrinsic energy transfer from the electron beam to the cluster can be considered as a unique possibility to investigate the transformation between energetically excited configurations of a specific cluster. This was exactly the idea behind a recent study that focused on the dynamical behavior of an ultra-small Ge clusters, consisting of less than 25 atoms. Aberration corrected HAADF STEM was used to acquire series of 2D images. From these series, specific frames were selected and analyzed using statistical parameter estimation theory. In this manner, the number of atoms at each position could be determined. In order to extend the 2D structural information that is available to 3D, ab initio calculations were carried out. As an input, different starting configurations, all in agreement with the experimental 2D HAADF STEM images, were used. All of the relaxed cluster configurations, illustrated in Fig. 7, stay relatively close to the input structures. However, only those configurations in which a planar base structure was assumed, were found to be still compatible with the 2D experimental images. In this manner, reliable 3D structural models are obtained for the ultra-small clusters.

7. Conclusions and outlook

Clearly, advanced electron tomography will take characterization of nanomaterials to a new level. This will lead to a better understanding and optimization of existing materials as well as the design of new structures with desired properties. Although several nanomaterials have been visualized atom by atom, new challenges are currently emerging. One of these goals is to visualize defects or interfaces with the same resolution as demonstrated so far. Next, the aim will be to measure not only the positions of the atoms in 3D, but also to determine the chemical nature and oxidation state atom by atom. Obviously, the achievement of atomic resolution in 3D should not be considered as the end of a quest, but as the start of a new journey in the field of 3D electron microscopy and materials science in general.

Acknowledgements

The authors gratefully acknowledge funding from the Research Foundation Flanders (FWO, Belgium). GVT and SB acknowledge the European Research Council under the 7th Framework Program (FP7), ERC grant No. 246791 – COUNTATOMS and ERC grant No. 335078 – COLOURATOMS. The authors would like to thank the colleagues who have contributed to this work, including K.J. Batenburg, E. Biermans, L. Molina-Luna, A. De Backer, R. Erni, M.D. Rossell, M. van Huis, D. Vanmaekelbergh, M. Casavola, W. Van den Broek, L. Manna, L. Liz-Marzán, E. Carbó-Argibay, S. Gómez-Graña, P. Lievens, M. Van Bael, B. Partoens and B. Schoeters.

References

[1] D.J. Derosier, A. Klug, Reconstruction of 3-dimensional structures from electron micrographs, Nature 217 (1968) 130–134.
[2] W. Hoppe, R. Langer, G. Knesch, C. Poppe, Protein crystal structure analysis with electron rays, Naturwissenschaften 55 (1968) 333–336.
[3] A. Leis, B. Rockel, L. Andrees, W. Baumeister, Visualizing cells at the nanoscale, Trends Biochem. Sci. 34 (2009) 60–70.
[4] K.B. Lu, E. Sourty, R. Guerra, G. Bar, J. Loos, Critical comparison of volume data obtained by different electron tomography techniques, Macromolecules 43 (2010) 1444–1448.
[5] P.W. Hawkes, The electron microscope as a structure projector, in: J. Frank (Ed.), Electron Tomography: Three-Dimensional Imaging with the Transmission Electron Microscope, Plenum Press, New York, 1992.
[6] R.J. Spontak, M.C. Williams, D.A. Agard, 3-Dimensional study of cylindrical morphology in a styrene butadiene styrene block copolymer, Polymer 29 (1988) 387–395.
[7] A.J. Koster, U. Ziese, A.J. Verkleij, A.H. Janssen, K.P. de Jong, Three-dimensional transmission electron microscopy: A novel imaging and characterization technique with nanometer scale resolution for materials science, J. Phys. Chem. B 104 (2000) 9368–9370.
[8] P.A. Midgley, M. Weyland, 3D electron microscopy in the physical sciences: the development of Z-contrast and EFTEM tomography, Ultramicroscopy 96 (2003) 413–431.
[9] M. Weyland, T.J.V. Yates, R.E. Dunin-Borkowski, L. Laffont, P.A. Midgley, Nanoscale analysis of three-dimensional structures by electron tomography, Scr. Mater. 55 (2006) 29–33.
[10] T.J.V. Yates, M. Weyland, L. Laffont, D. Zhi, R.E. Dunin-Borkowski, P.A. Midgley, 3D analysis of semiconductor structures using STEM tomography, in: Microscopy of Semiconducting Materials 2003, 2003, pp. 541–544.
[11] D. Wolf, A. Lubk, H. Lichte, H. Friedrich, Towards automated electron holographic tomography for 3D mapping of electrostatic potentials, Ultramicroscopy 110 (2010) 390–399.
[12] M. Bar Sadan, L. Houben, S.G. Wolf, A. Enyashin, G. Seifert, R. Tenne, K. Urban, Toward atomic-scale bright-field electron tomography for the study of fullerene-like nanostructures, Nano Lett. 8 (2008) 891–896.
[13] Y. Li, H. Tan, X.Y. Yang, B. Goris, J. Verbeeck, S. Bals, P. Colson, R. Cloots, G. Van Tendeloo, B.L. Su, Well shaped MnO nano-octahedra with anomalous magnetic behavior and enhanced photodecomposition properties, Small 7 (2011) 475–483.
[14] B. Goris, S. Bals, W. Van den Broek, J. Verbeeck, G. Van Tendeloo, Exploring different inelastic projection mechanisms for electron tomography, Ultramicroscopy 111 (2011) 1262–1267.
[15] G. Mobus, R.C. Doole, B.J. Inkson, Spectroscopic electron tomography, Ultramicroscopy 96 (2003) 433–451.
[16] M.H. Gass, K.K.K. Koziol, A.H. Windle, P.A. Midgley, Four-dimensional spectral tomography of carbonaceous nanocomposites, Nano Lett. 6 (2006) 376–379.
[17] S. Bals, G. Van Tendeloo, C. Kisielowski, A new approach for electron tomography: Annular dark-field transmission electron microscopy, Adv. Mater. 18 (2006) 892–895.
[18] R.A. Crowther, D.J. Derosier, A. Klug, Reconstruction of 3 dimensional structure from projections and its application to electron microscopy, Proc. R. Soc. Lond., Ser. A 317 (1970) 319–340.
[19] P. Gilbert, Iterative methods for 3-dimensional reconstruction of an object from projections, J. Theor. Biol. 36 (1972) 105–117.
[20] I. Arslan, J.R. Tong, P.A. Midgley, Reducing the missing wedge: High-resolution dual axis tomography of inorganic materials, Ultramicroscopy 106 (2006) 994–1000.
[21] J. Tong, I. Arslan, P. Midgley, A novel dual-axis iterative algorithm for electron tomography, J. Struct. Biol. 153 (2006) 55–63.
[22] N. Kawase, M. Kato, H. Nishioka, H. Jinnai, Transmission electron microtomography without the "missing wedge" for quantitative structural analysis, Ultramicroscopy 107 (2007) 8–15.
[23] E. Biermans, L. Molina, K.J. Batenburg, S. Bals, G. Van Tendeloo, Measuring porosity at the nanoscale by quantitative electron tomography, Nano Lett. 10 (2010) 5014–5019.
[24] X.X. Ke, S. Bals, D. Cott, T. Hantschel, H. Bender, G. Van Tendeloo, Three-dimensional analysis of carbon nanotube networks in interconnects by electron tomography without missing wedge artifacts, Microsc. Microanal. 16 (2010) 210–217.
[25] L. Molina, H.Y. Tan, E. Biermans, K.J. Batenburg, J. Verbeeck, S. Bals, G. Van Tendeloo, Barrier efficiency of sponge-like $La_2Zr_2O_7$ buffer layers for YBCO-coated conductors, Supercond. Sci. Technol. 24 (2011).
[26] K. Jarausch, D.N. Leonard, Three-dimensional electron microscopy of individual nanoparticles, J. Electron Microsc. 58 (2009) 175–183.
[27] H. Jinnai, Y. Nishikawa, R.J. Spontak, S.D. Smith, D.A. Agard, T. Hashimoto, Direct measurement of interfacial curvature distributions in a bicontinuous block copolymer morphology, Phys. Rev. Lett. 84 (2000) 518–521.
[28] Y. Ikeda, A. Katoh, J. Shimanuki, S. Kohjiya, Nano-structural observation of in situ silica in natural rubber matrix by three dimensional transmission electron microscopy, Macromol. Rapid Commun. 25 (2004) 1186–1190.
[29] L. Laffont, M. Weyland, R. Raja, J.M. Thomas, P.A. Midgley, Electron tomography of heterogeneous catalysts, Inst. Phys. Conf. Ser. (2004) 459–462.
[30] L. Houben, M. Bar Sadan, Refinement procedure for the image alignment in high-resolution electron tomography, Ultramicroscopy 111 (2011) 1512–1520.
[31] W. Van den Broek, A. Rosenauer, B. Goris, G. Martinez, S. Bals, S. Van Aert, D. Van Dyck, Correction of non-linear thickness effects in HAADF STEM electron tomography, Ultramicroscopy 116 (2012) 8–12.
[32] T. Altantzis, B. Goris, A. Sánchez-Iglesias, M. Grzelczak, L.M. Liz-Marzán, S. Bals, Quantitative structure determination of large three-dimensional nanoparticle assemblies, Part. Part. Syst. Charact. 30 (2013) 84–88.
[33] W. van Aarle, K.J. Batenburg, J. Sijbers, Optimal threshold selection for segmentation of dense homogeneous objects in tomographic reconstructions, IEEE Trans. Med. Imaging 30 (2011) 980–989.
[34] S. Bals, K.J. Batenburg, J. Verbeeck, J. Sijbers, G. Van Tendeloo, Quantitative three-dimensional reconstruction of catalyst particles for bamboo-like carbon nanotubes, Nano Lett. 7 (2007) 3669–3674.
[35] K.J. Batenburg, S. Bals, J. Sijbers, C. Kubel, P.A. Midgley, J.C. Hernandez, U. Kaiser, E.R. Encina, E.A. Coronado, G. Van Tendeloo, 3D imaging of nanomaterials by discrete tomography, Ultramicroscopy 109 (2009) 730–740.

[36] S. Bals, K.J. Batenburg, D.D. Liang, O. Lebedev, G. Van Tendeloo, A. Aerts, J.A. Martens, C.E.A. Kirschhock, Quantitative three-dimensional modeling of zeotile through discrete electron tomography, J. Am. Chem. Soc. 131 (2009) 4769–4773.
[37] B. Goris, W. Van den Broek, K.J. Batenburg, H.H. Mezerji, S. Bals, Electron tomography based on a total variation minimization reconstruction technique, Ultramicroscopy 113 (2012) 120–130.
[38] Z. Saghi, D.J. Holland, R. Leary, A. Falqui, G. Bertoni, A.J. Sederman, L.F. Gladden, P.A. Midgley, Three-dimensional morphology of iron oxide nanoparticles with reactive concave surfaces. A compressed sensing-electron tomography (CS-ET) approach, Nano Lett. 11 (2011) 4666–4673.
[39] J.M. Zielinski, M.S. Vratsanos, J.H. Laurer, R.J. Spontak, Phase-separation studies of heat-cured ATU-flexibilized epoxies, Polymer 37 (1996) 75–84.
[40] B. Goris, T. Roelandts, J. Batenburg, H. Heidari Mezerji, S. Bals, Advanced reconstruction algorithms for electron tomography: from comparison to combination, Ultramicroscopy 127 (2012) 40–47.
[41] A. Alpers, R.J. Gardner, S. Konig, R.S. Pennington, C.B. Boothroyd, L. Houben, R.E. Dunin-Borkowski, K.J. Batenburg, Geometric reconstruction methods for electron tomography, Ultramicroscopy 128 (2013) 42–54.
[42] Z. Saghi, X.J. Xu, G. Mobus, Model based atomic resolution tomography, J. Appl. Phys. 106 (2009).
[43] J.R. Jinschek, K.J. Batenburg, H.A. Calderon, R. Kilaas, V. Radmilovic, C. Kisielowski, 3-D reconstruction of the atomic positions in a simulated gold nanocrystal based on discrete tomography: Prospects of atomic resolution electron tomography, Ultramicroscopy 108 (2008) 589–604.
[44] S. Van Aert, K.J. Batenburg, M.D. Rossell, R. Erni, G. Van Tendeloo, Three-dimensional atomic imaging of crystalline nanoparticles, Nature 470 (2011) 374–377.
[45] S. Bals, M. Casavola, M.A. van Huis, S. Van Aert, K.J. Batenburg, G. Van Tendeloo, D. Vanmaekelbergh, Three-dimensional atomic imaging of colloidal core–shell nanocrystals, Nano Lett. 11 (2011) 3420–3424.
[46] M.C. Scott, C.C. Chen, M. Mecklenburg, C. Zhu, R. Xu, P. Ercius, U. Dahmen, B.C. Regan, J.W. Miao, Electron tomography at 2.4-angstrom resolution, Nature 483 (2012) 444–447.
[47] D. Van Dyck, F.R. Chen, Big-Bang tomography as a new route to atomic resolution electron tomography, Nature 486 (2012) 243–246.
[48] S. Van Aert, A. De Backer, G.T. Martinez, B. Goris, S. Bals, G. Van Tendeloo, A. Rosenauer, Procedure to count atoms with trustworthy single-atom sensitivity, Phys. Rev. B 87 (2013).
[49] E. Lee, B.P. Fahimian, C.V. Iancu, C. Suloway, G.E. Murphy, E.R. Wright, D. Castano-Diez, G.J. Jensen, J.W. Miao, Radiation dose reduction and image enhancement in biological imaging through equally-sloped tomography, J. Struct. Biol. 164 (2008) 221–227.
[50] C.C. Chen, C. Zhu, E.R. White, C.Y. Chiu, M.C. Scott, B.C. Regan, L.D. Marks, Y. Huang, J. Miao, Three-dimensional imaging of dislocations in a nanoparticle at atomic resolution, Nature 496 (2013) 74–77.
[51] B. Goris, S. Bals, W. Van den Broek, E. Carbo-Argibay, S. Gomez-Grana, L.M. Liz-Marzán, G. Van Tendeloo, Atomic-scale determination of surface facets in gold nanorods, Nat. Mater. 11 (2012) 930–935.
[52] S.J. Kim, K. Koh, M. Lustig, S. Boyd, D. Gorinevsky, An interior-point method for large-scale l(1)-regularized least squares, IEEE J. Sel. Top. Signal Process. 1 (2007) 606–617.
[53] B. Goris, A. de Backer, S. Van Aert, S. Gomez-Grana, L.M. Liz-Marzan, G. Van Tendeloo, S. Bals, 3D elemental mapping at the atomic scale in bimetallic nanocrystals, Nano Lett. 13 (2013) 4236–4241.
[54] K. van Benthem, A.R. Lupini, M. Kim, H.S. Baik, S. Doh, J.H. Lee, M.P. Oxley, S.D. Findlay, L.J. Allen, J.T. Luck, S.J. Pennycook, Three-dimensional imaging of individual hafnium atoms inside a semiconductor device, Appl. Phys. Lett. 87 (2005).
[55] H.L.L. Xin, D.A. Muller, Prospects for reliable 3D imaging in aberration-corrected STEM, TEM and SCEM, Microsc. Microanal. 15 (2009) 1474–1475.
[56] W. Van den Broek, S. Van Aert, D. Van Dyck, A model based reconstruction technique for depth sectioning with scanning transmission electron microscopy, Ultramicroscopy 110 (2010) 548–554.
[57] E.C. Cosgriff, P.D. Nellist, A.J. D'Alfonso, S.D. Findlay, G. Behan, P. Wang, L.J. Allen, A.I. Kirkland, Image contrast in aberration-corrected scanning confocal electron microscopy, Adv. Imaging Electron Phys. 162 (162) (2010) 45–76.
[58] P.D. Nellist, G. Behan, A.I. Kirkland, C.J.D. Hetherington, Confocal operation of a transmission electron microscope with two aberration correctors, Appl. Phys. Lett. 89 (2006).
[59] P. Wang, G. Behan, M. Takeguchi, A. Hashimoto, K. Mitsuishi, M. Shimojo, A.I. Kirkland, P.D. Nellist, Nanoscale energy-filtered scanning confocal electron microscopy using a double-aberration-corrected transmission electron microscope, Phys. Rev. Lett. 104 (2010).
[60] P. Ercius, D. Muller, Incoherent bright field STEM for imaging and tomography of ultra-thick TEM cross-sections, Microsc. Microanal. 15 (2009) 238–239.
[61] U. Kaiser, A. Chuvilin, Enhanced compositional contrast in imaging of nanoprecipitates buried in a defective crystal using a conventional TEM, Microsc. Microanal. 9 (2003) 36–41.
[62] J.M. Rebled, L. Yedra, S. Estrade, J. Portillo, F. Peiro, A new approach for 3D reconstruction from bright field TEM imaging: beam precession assisted electron tomography, Ultramicroscopy 111 (2011) 1504–1511.
[63] J.S. Barnard, J. Sharp, J.R. Tong, P.A. Midgley, High-resolution three-dimensional imaging of dislocations, Science 313 (2006) 319.
[64] G. Mobus, B.J. Inkson, Nanoscale tomography in materials science, Mater. Today 10 (2007) 18–25.
[65] R.D. Leapman, E. Kocsis, G. Zhang, T.L. Talbot, P. Laquerriere, Three-dimensional distributions of elements in biological samples by energy-filtered electron tomography, Ultramicroscopy 100 (2004) 115–125.
[66] A. Yurtsever, M. Weyland, D.A. Muller, Three-dimensional imaging of nonspherical silicon nanoparticles embedded in silicon oxide by plasmon tomography, Appl. Phys. Lett. 89 (2006).
[67] O. Nicoletti, R. Leary, F. de la Pena, D.J. Holland, C. Ducati, P. Midgley, Three-dimensional imaging of localized surface plasmon resonances of metal nanoparticles, in: EMC 2012, Manchester, 2012.
[68] A.C. Twitchett-Harrison, T.J.V. Yates, S.B. Newcomb, R.E. Dunin-Borkowski, P.A. Midgley, High-resolution three-dimensional mapping of semiconductor dopant potentials, Nano Lett. 7 (2007) 2020–2023.
[69] C. Phatak, M. Beleggia, M. De Graef, Vector field electron tomography of magnetic materials: Theoretical development, Ultramicroscopy 108 (2008) 503–513.
[70] S.J. Lade, D. Paganin, M.J. Morgan, Electron tomography of electromagnetic fields, potentials and sources, Opt. Commun. 253 (2005) 392–400.
[71] C. Phatak, A.K. Petford-Long, M. De Graef, Three-dimensional study of the vector potential of magnetic structures, Phys. Rev. Lett. 104 (2010).
[72] M. Hytch, F. Houdellier, F. Hue, E. Snoeck, Nanoscale holographic interferometry for strain measurements in electronic devices, Nature 453 (2008) 1086–1089.
[73] M.J. Hytch, E. Snoeck, R. Kilaas, Quantitative measurement of displacement and strain fields from HREM micrographs, Ultramicroscopy 74 (1998) 131–146.
[74] B. Goris, M.A. Van Huis, S. Bals, H.W. Zandbergen, L. Manna, G. Van Tendeloo, Thermally induced structural and morphological changes of CdSe/CdS octapods, Small 8 (2012) 937–942.
[75] Z.Y. Li, N.P. Young, M. Di Vece, S. Palomba, R.E. Palmer, A.L. Bleloch, B.C. Curley, R.L. Johnston, J. Jiang, J. Yuan, Three-dimensional atomic-scale structure of size-selected gold nanoclusters, Nature 451 (2008) 46–48.